Supplementary Material (SM) for:

Numerical simulation and parametric sensitivity study of titanium dioxide particles synthesised in a stagnation flame

Casper S. Lindberg[a,b], Manoel Y. Manuputty[a,b], Philipp Buerger[a], Jethro Akroyd[a,b], Markus Kraft[a,b,c,*]

[a] *Department of Chemical Engineering and Biotechnology, University of Cambridge, Philippa Fawcett Drive, Cambridge, CB3 0AS, United Kingdom*

[b] *CARES, Cambridge Centre for Advanced Research and Education in Singapore, 1 Create Way, CREATE Tower, #05-05, Singapore, 138602*

[c] *School of Chemical and Biomedical Engineering, Nanyang Technological University, 62 Nanyang Drive, Singapore, 637459*

1. Flame measurements

Temperature measurements. The flame temperature profile was measured using a thin wire thermocouple (d = 75 μm, S-type, P10R-003, Omega Engineering) scanned along the flow direction with a motorised translational stage (Velmex). The scan speed was set to 0.5 mm/s in order to ensure a near steady-state measurement of the temperature. Due to deposition of particles on the wire when the precursor (TTIP) is used, this method is only suitable for undoped flames. Additionally, the maximum operating temperature is limited by the melting point of the thermocouple material (2041 K for Pt). Thus, the temperature measurement could only be performed for the lean flame (ϕ = 0.35, T_{ad} = 2073 K), as the rich flame temperature was too high ($\phi = 1.67$, $T_{\mathrm{ad}} = 2542$ K) [4].

As the flame is stabilised by stretch (aerodynamically), the thermocouple wire easily "catches" or becomes the anchor point for the flame when the thermocouple wire is near the flame front (upstream). It was found that this could be minimised by placing the thermocouple off-centre, approximately 3 mm from the centreline. In this condition, the flame disturbance is not observable compared to the pre-existing fluctuations of the flame front. Two assumptions are made here: (1) the temperature is radially uniform at least up to 3 mm from the centre which is reasonable given the flame diameter is roughly 3 cm and (2) the flame curvature is negligible and thus the flame front at 3 mm is taken to be the same as that at the centreline.

The actual flame temperature, T, is calculated from the measured temperature, T_{tc}, by taking into account the convective-radiative heat transfer of the thermocouple wire [7], i.e. "radiation correction".

*Corresponding author
Email address: mk306@cam.ac.uk (Markus Kraft)

Assuming a steady-state, this is given as

$$T = T_{\mathrm{tc}} + \epsilon_{\mathrm{tc}}\sigma\left(T_{\mathrm{tc}}^4 - T_0^4\right)\frac{d_j}{k_g \mathrm{Nu}}, \tag{1}$$

where ϵ_{tc} is the thermocouple emissivity, σ is the Stefan-Boltzmann radiation constant, T_0 is the radiative sink temperature (surrounding temperature, 300 K), d_j is the thermocouple junction diameter (0.24 mm [5]), k_g is the average gas thermal conductivity, and Nu is the thermocouple junction Nusselt number. The emissivity of the thermocouple (S-type, Pt/10%Rh-Pt) is given as a function of temperature as reported by Shaddix [7],

$$\epsilon_{\mathrm{tc}} = -0.1 + 3.24 \times 10^{-4} T - 1.25 \times 10^{-7} T^2 + 2.18 \times 10^{-11} T^3. \tag{2}$$

The Nusselt number is calculated using the correlation for low Reynold number, Re, forced flow over a sphere as follows [6],

$$\mathrm{Nu} = 2 + 0.6 \mathrm{Re}^{1/2} \mathrm{Pr}^{1/3}, \tag{3}$$

where Re is calculated based on the thermocouple junction diameter, i.e. $\mathrm{Re} = \rho_g u_g d_j / \mu_g$, Pr is the gas Prandtl number, i.e. $\mathrm{Pr} = c_p \mu_g / k_g$. ρ_g, u_g, μ_g, and c_p are the mass density, velocity, dynamic viscosity, and specific heat of the gas phase, respectively. These and the average gas thermal conductivity, k_g, were obtained from the simulated gas species and velocity profiles with the energy equation solved for the flame mixture using the *k*inetics® software package [1, 3]. The boundary conditions in the simulation are adjusted (see Table 1) to match the position at which the temperature rises sharply. It is noted that this point (approximately 3.5 mm from the surface) is not affected by the radiation correction as shown in Fig. S1.

Figure S1 shows the temperature profiles, before and after the radiation correction, for the undoped lean flame. The thermocouple measurement is able to capture the high temperature gradient at the edge of the combustion zone expected for a stretch stabilised stagnation flame. An uncertainty of ±50 K is assigned to the temperature profiles due to the uncertainty in the parameters and estimated transport properties used for the correction [5, 7]. In addition, an estimated uncertainty of ±0.2 mm is assigned due to the fluctuation of the flame front during the experiment.

Flame images. Photographs of the undoped flames were taken with a digital camera (EX-ZR5000, Casio) in order to estimate the flame standing distance. This is needed because no temperature data for the rich flame ($\phi = 1.67$) was available. The photographs were taken with 20 ms exposure time and the data averaged over 4 photographs for each flame. Figure S2 shows the averaged intensities (blue channel) along the burner centreline for the lean and rich flames. Herein the flame distance is approximated as the distance (upstream from the flame) at which the intensity is half of the maximum intensity as annotated in Fig. S2.

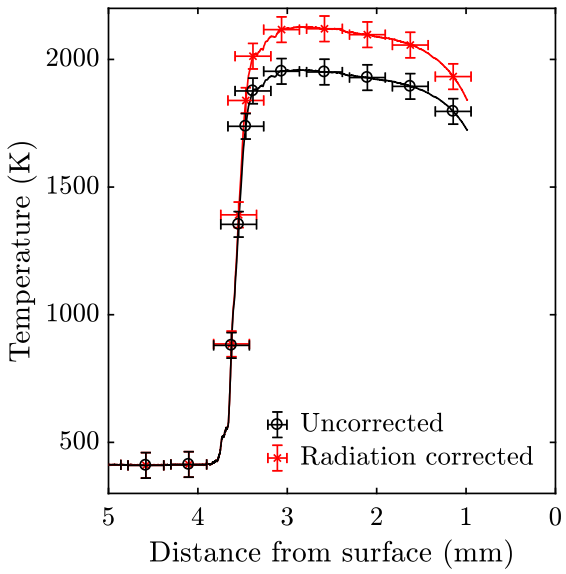

Figure S1: The temperature profiles, before and after the radiation correction, of the $\phi = 0.35$ undoped flame. The lines represent all data points while the symbols are every 240th points. The errorbars represent ± 0.2 mm and ± 50 K uncertainties.

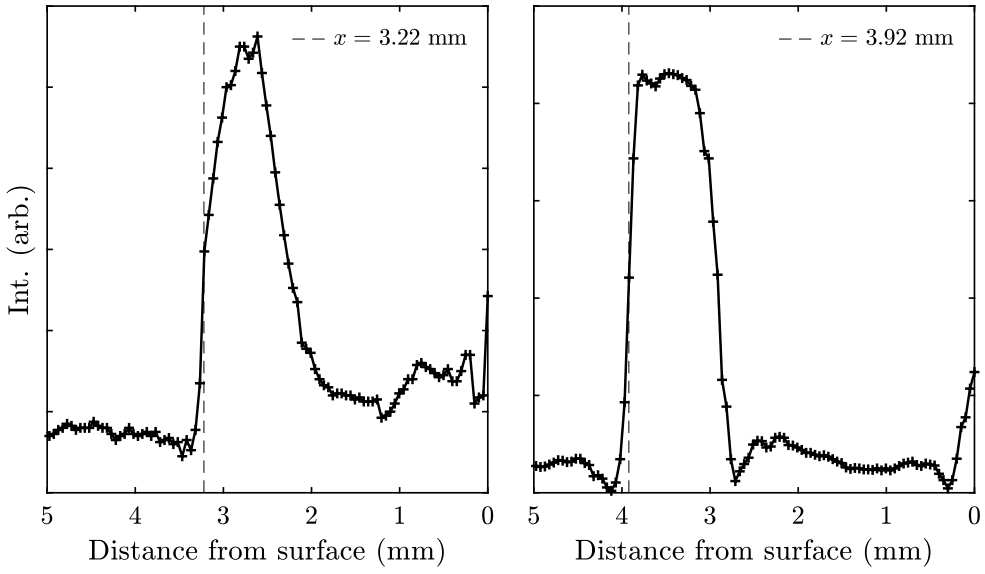

Figure S2: The blue channel intensities from the flame photographs along the burner centreline for the lean ($\phi = 0.35$, left) and rich flames ($\phi = 1.67$, right). The vertical dashed lines denote the distance at which the intensity is half of the maximum intensity, herein defined as the flame standing distance.

2. Simulated flame profiles

The simulated flame temperature and H mole fraction profiles from the first-step simulation for varying TTIP loading rates and flame equivalence ratios used in this work are shown in Fig. S3. In addition, Fig. S4 shows the simulated profiles for flames with varying flame standing distance, here defined as the location of

maximum H mole fraction. The variation of ±0.2 mm is assigned to take into account the flame fluctuation as well as the uncertainty from the assumptions made for the flame standing distance used in this work.

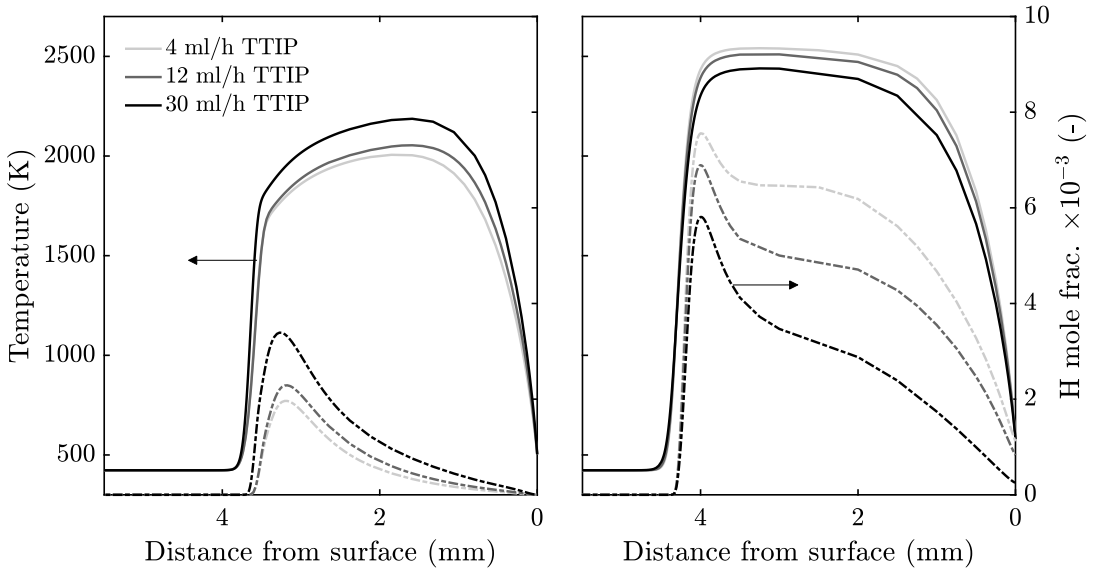

Figure S3: The simulated temperature and H mole fraction profiles for the lean ($\phi = 0.35$, left) and rich flames ($\phi = 1.67$, right) with varying precursor loading rate. Particle model parameters used: $\epsilon = 2.64$, $\rho = \rho_{\text{anatase}}$.

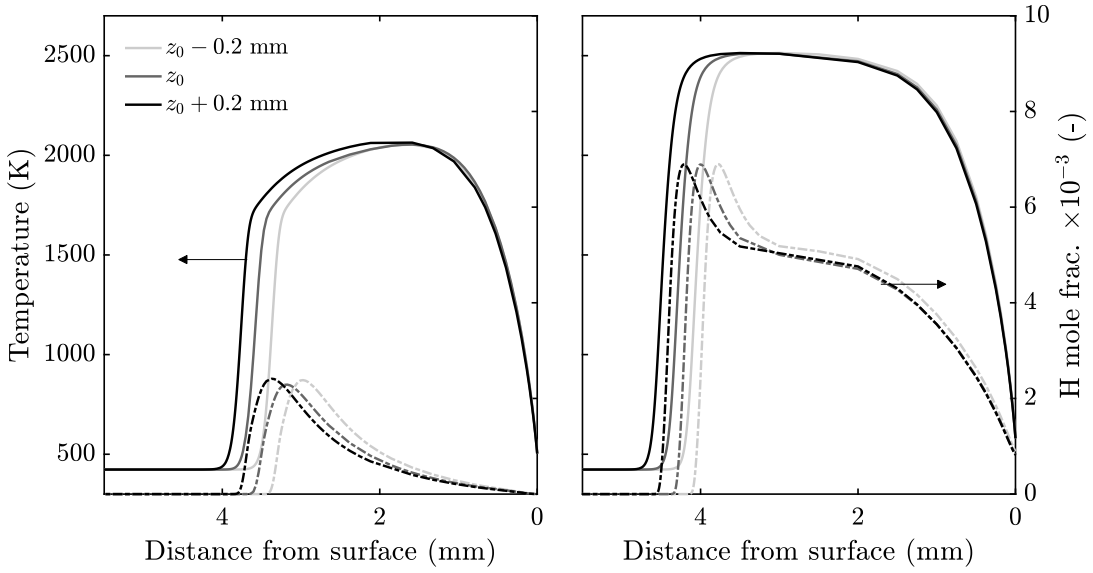

Figure S4: The simulated temperature and H mole fraction profiles for the lean ($\phi = 0.35$, left) and rich flames ($\phi = 1.67$, right) with 12 ml/h TTIP loading and varying flame distances, $z = z_0 \pm 0.2$ mm (z_0 is the reference flame distance from Fig. S2). Particle model parameters used: $\epsilon = 2.64$, $\rho = \rho_{\text{anatase}}$.

The $Ti(OH)_4$ mole fraction is plotted in Fig. S5 for both lean and rich flames with 12 ml/h TTIP loading

and surface growth efficiencies $\gamma_{sg} = 1$ and $\gamma_{sg} = 0.01$. The lean flame with $\gamma_{sg} = 0.01$ shows unreacted $Ti(OH)_4$ near the stagnation surface.

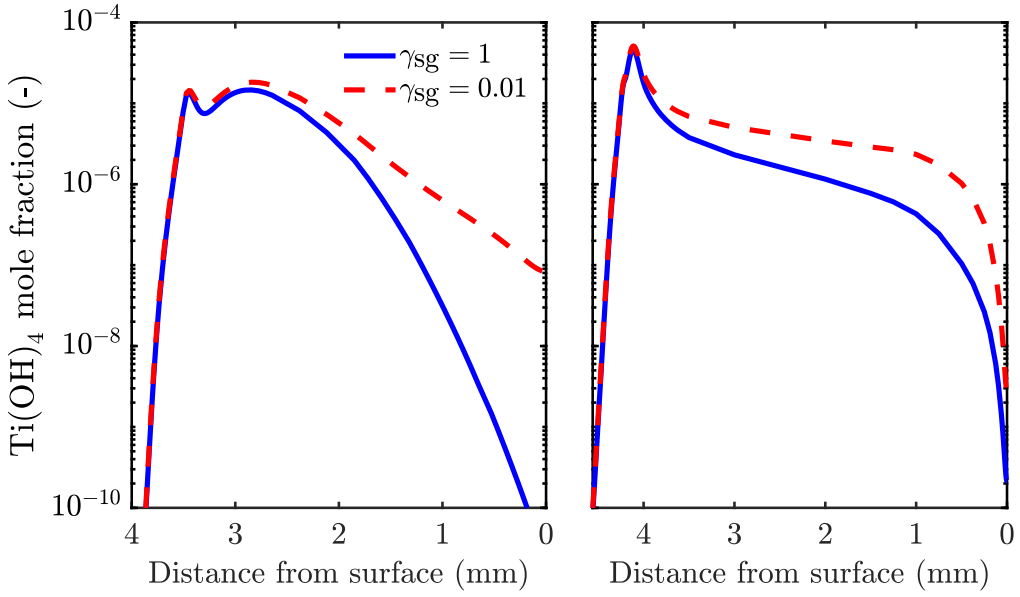

Figure S5: Simulated $Ti(OH)_4$ mole fraction for the lean flame ($\phi = 0.35$, left) and rich flame ($\phi = 1.67$, right) at 12 ml/h TTIP loading, with $\gamma_{sg} = 0.01$ and $\gamma_{sg} = 1$.

3. Parametric sensitivity

Collision enhancement factor. The sensitivities of the primary and aggregate mean diameter and coefficient of variation (CV) to the collision enhancement factor ϵ are shown in Fig. S6. ϵ is applied as a multiplicative factor to the free molecular kernels for all collision processes in the particle model; namely, inception, surface growth and coagulation. The enhancement factor is varied in the range: $\epsilon = 2.2 - 3.0$. The base case value is taken as $\epsilon = 2.64$ as per Manuputty et al. [3], based on the value calculated by Zhang et al. [8]. $\epsilon = 2.2$ is the size-independent enhancement factor due to van der Waals forces calculated by Harris and Kennedy [2] for spherical soot particles. The morphological descriptors are not particularly sensitive over the range of ϵ studied. The mean primary and aggregate diameters show a slight increase with increasing ϵ, as would be expected from larger collision rates. The primary and aggregate CVs are largely insensitive to ϵ.

Density. Figure S6 shows the sensitivity of the primary and aggregate mean diameter and coefficient of variation (CV) to the particle density: $\rho = 3.84$ g/cm^3 (anatase) and $\rho = 4.25$ g/cm^3 (rutile). It is important to note that we are actually imposing an effective ρ for particles of all sizes at all stages of evolution. Although the particles collected are anatase and rutile in the lean and rich flames respectively, the incipient particles are likely to have significantly lower density, which might affect the results. Overall,

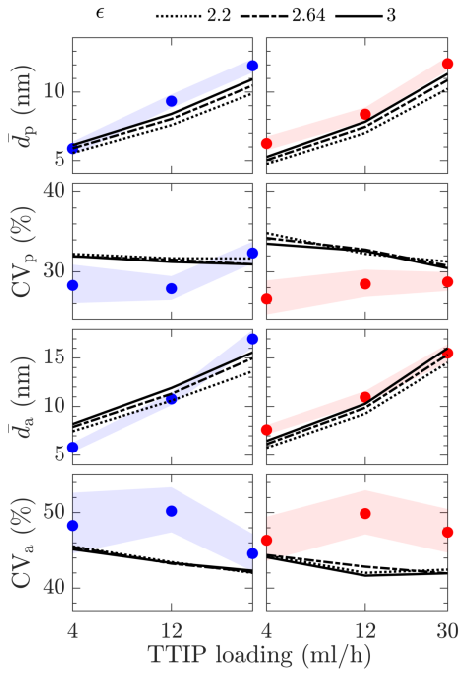

Figure S6: Sensitivity of the primary and aggregate mean diameter and coefficient of variation (CV) to the molecular enhancement factor ϵ for lean ($\phi = 0.35$, left panels) and rich ($\phi = 1.67$, right panels) flames. The shaded areas indicate estimated uncertainty bounds of the experimental measurements.

the descriptors are not very sensitive to the choice of density. As expected, a lower density (anatase) yields larger mean diameters.

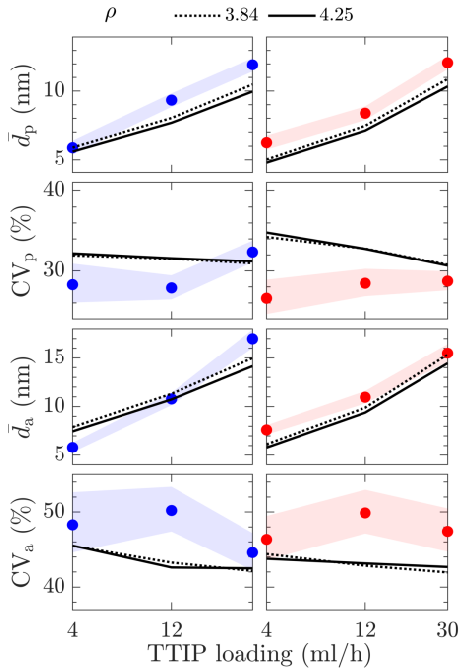

Figure S7: Sensitivity of the primary and aggregate mean diameter and coefficient of variation to the particle density $\rho = 3.84$ g/cm^3 (anatase, base case), 4.25 g/cm^3 (rutile) for lean ($\phi = 0.35$, left panels) and rich ($\phi = 1.67$, right panels) flames. The shaded areas indicate estimated uncertainty bounds of the experimental measurements.

References

[1] CMCL Innovations, 2016. *k*inetics®. URL: http://www.cmclinnovations.com/.

[2] Harris, S.J., Kennedy, I.M., 1988. The coagulation of soot particles with van der Waals forces. Combust. Sci. Technol. 59, 443–454. doi:10.1080/00102208808947110.

[3] Manuputty, M.Y., Akroyd, J., Mosbach, S., Kraft, M., 2017. Modelling TiO_2 formation in a stagnation flame using method of moments with interpolative closure. Combust. Flame 178, 135–147. doi:10.1016/j.combustflame.2017.01.005.

[4] Manuputty, M.Y., Lindberg, C.S., Botero, M.L., Akroyd, J., Kraft, M., 2019. Detailed characterisation of TiO_2 nanoaggregate morphology using TEM image analysis. J. Aerosol Sci. 133, 96–112. doi:10.1016/j.jaerosci.2019.04.012.

[5] McEnally, C.S., Köylü, Ü.Ö., Pfefferle, L.D., Rosner, D.E., 1997. Soot volume fraction and temperature measurements in laminar nonpremixed flames using thermocouples. Combust. Flame 109, 701–720. doi:10.1016/S0010-2180(97)00054-0.

[6] Ranz, W.E., Marshall, W.R.J., 1952. Evaporation from drops. Chem. Eng. Prog. 48, 141–146.

[7] Shaddix, C.R., 1999. Correcting thermocouple measurements for radiation loss: a critical review. Proc. 33rd Natl. Heat Transf. Conf. .

[8] Zhang, Y., Li, S., Yan, W., Yao, Q., Tse, S.D., 2011. Role of dipole-dipole interaction on enhancing Brownian coagulation of charge-neutral nanoparticles in the free molecular regime. J. Chem. Phys. 134, 084501. doi:10.1063/1.3555633.